ELSEVIER

Journal of Nuclear Materials 266–269 (1999) 771–776

journal of nuclear materials

Particle diffusion coefficient at the edge of RFX

M. Bagatin [a,b,*], V. Antoni [a,b], D. Desideri [c], E. Martines [a], R. Pasqualotto [a], R. Pugno [c], G. Serianni [a], L. Tramontin [a], M. Valisa [a]

[a] *Consorzio RFX, Corso Stati Uniti, 4-35127 Padova, Italy*
[b] *INFM, Unita'd: Padova Sez. A, Via Marzolo, 8-35131 Padova, Italy*
[c] *Dipartimento Ingegneria Elettrica, Via Gradenigo, 6a-35131 Padova, Italy*

Abstract

The radial particle diffusion coefficient D of the RFP experiment RFX has been derived from particle balance in the local scrape-off layer created by an instrumented limiter inserted into the edge region. The parallel particle flux incident on the limiter and its spatial decay are measured by Langmuir probes, whereas the connection lengths between the limiter and the wall are inferred from the images of a CCD camera with a H_α and N II filter, and ion sources are taken into account. The measured values of D are in the range 10–20 m^2/s for plasma current in the range 300–400 kA. The radial profile of D exhibits a maximum close to the wall and it decreases to lower values at r/a around 0.90. The value of D and its profile at the edge appear to be consistent with those derived from the electrostatic turbulence driven particle flux and from the local density profile. The results are discussed in terms of the diffusion mechanism in the edge plasma and in the scrape-off layer, by assessing the perturbation produced by the limiter insertion. © 1999 Elsevier Science B.V. All rights reserved.

Keywords: Diffusion; Edge transport; RFX; SOL modeling

1. Introduction

Particle transport is a key issue in magnetically confined plasmas and in recent years a detailed investigation of the mechanisms underlying this process has been undertaken in plasmas confined in reversed field pinch configuration (RFP). It has been found that in this configuration particle transport at the edge is anomalous and mostly driven by electrostatic turbulence at the edge [1]. This issue has a peculiar interest in RFP experiments since it strongly affects the global particle confinement. RFX is a large RFP device ($R = 2$ m, $a = 0.457$ m) designed to reach a plasma current of 2 MA [2]. In RFX the density profiles are found to be flat or hollow in the core [3], with steep density gradients in the edge region, where the ionisation source is located. The RFX device has no protruding limiters, but an armour of graphite tiles protecting almost 90% of the vessel surface [4]. As in most RFPs, it has been found that the parallel energy flux is non-isotropic. An asymmetry equal or larger than a factor of two is routinely measured at the edge between the parallel and antiparallel directions along the magnetic field, which has been associated to a flow of superthermal electrons [5]. When an object is inserted into the plasma, an electron drift side is identified corresponding to the direction whence superthermal electrons come.

The horizontal position of the plasma column can be controlled by an active vertical field. In the present campaign the toroidal shift during the current flat-top has been kept at 20–25 mm outwards, so as to make the outer region of the wall behave like a toroidal limiter. Therefore the perturbation produced by a limiter inserted from the outer equatorial plane can be more conveniently characterised by a collection length, rather than by a connection length.

The aim of this paper is to present the diffusion coefficient derived from the particle balance in the scrape off layer (SOL) originated by an insertable limiter and to compare it with that obtained from electrostatic

* Corresponding author. Tel.: +39-049 829 5023; fax: +39-049 870 0718; e-mail: bagatin@igi.pd.cnr.it.

0022-3115/99/$ – see front matter © 1999 Elsevier Science B.V. All rights reserved.
PII: S0022-3115(98)00603-5

turbulence, in order to test the anomalous nature of particle transport. Both values are then compared with the Bohm estimate.

2. Experimental setup

The diagnostic layout is shown in the top view of Fig. 1. A limiter equipped with Langmuir probes has been inserted in the equatorial plane from the outboard side, up to 60 mm inside the plasma. A schematic view of the limiter is depicted in Fig. 2. The insertion of this limiter produces a local SOL which extends along both drift sides. It is defined as the region outside the last closed flux surface (LCFS) determined by the plasma limiter contact. In the RFP configuration the toroidal magnetic field strength at the edge is about 1/5 to 1/10 of the poloidal component, so that the SOL extends almost along the poloidal direction, as the angle of the total magnetic field with respect to the poloidal direction is 6–10°. Since the SOL thickness is much shorter than the minor radius a, the volume delimited by the limiter shadow on the ion drift side can be represented in slab geometry, as sketched in the rectified poloidal section of Fig. 2. The width and height of the limiter, w and l, and the collection length L_c are also shown on the figure.

The limiter, described in Ref. [6], is equipped with three different arrays of flush mounted electrodes on a boron nitride body, which can be arranged in different Langmuir probe configurations. In the present campaign two probes of the central array (Fig. 2) have been used. They are referred to as probe 1, located at 2 mm from the leading edge of the limiter, and probe 3, located 7 mm radially outward from probe 1. The plasma current in this experimental campaign has been kept at values lower than 400 kA, in order to limit the power loading.

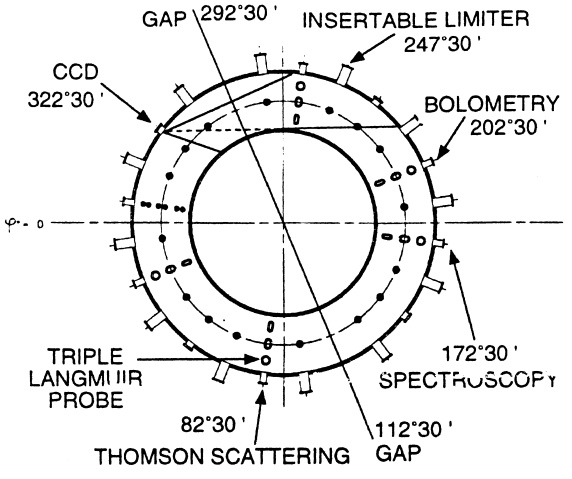

Fig. 1. Scheme of the experimental setup.

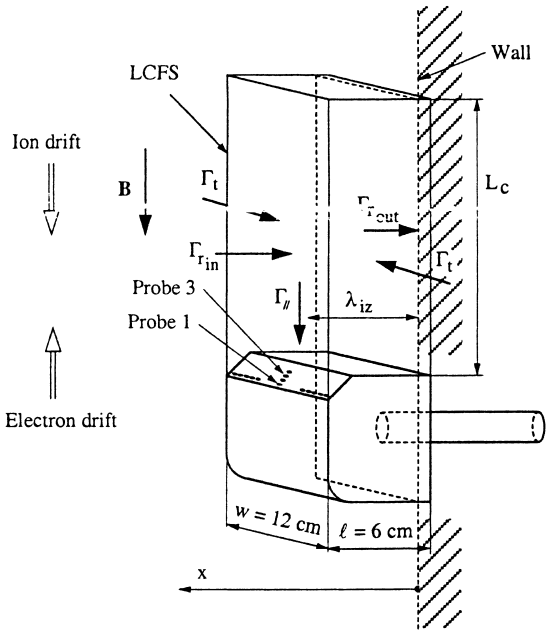

Fig. 2. Schematic of the SOL in the limiter shadow in slab geometry (not to scale).

The limiter has been oriented in such a way as to keep the instrumented side facing the ion drift side, where no significant superthermal tail is observed.

The insertion of the limiter into the plasma was monitored by a CCD camera located on the equatorial plane 90° apart and equipped with an interference filter with a transmission function centered on the H_α line (656 nm) but large enough (±6.5 nm) as to include several B I and N II lines [7]. Thanks to a stainless steel mirror placed inside the diagnostic port, the resulting view is wide enough so as to allow monitoring of the radiation emission in the shadow of the limiter. The 768 × 576 pixels image permits to resolve roughly 2 mm in the limiter region with the magnification used for these observations. The field of view of the CCD camera is shown in Fig. 1.

In order to test the reliability of this intrusive experimental technique, a preliminary appraisal of the perturbation has been performed by comparing two sets of similar discharges at toroidal current of 300–400 kA, respectively with the limiter inserted and withdrawn. The comparison has been made in terms of power balance, electron temperature and density, as well as edge particle flux.

With the limiter inserted 60 mm inside the plasma, the average input power during the current flat top rises by less than 10%, from 17 up to 18.2 MW, so that the fraction of radiated power in the perturbed discharges, as measured by bolometric tomography, increases from the standard 10% in unperturbed discharges to almost

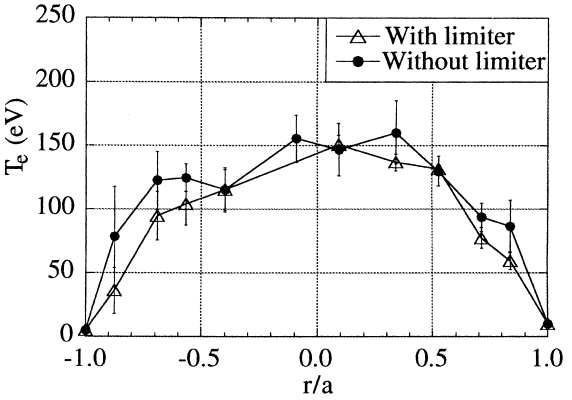

Fig. 3. Profile of electron temperature with and without limiter.

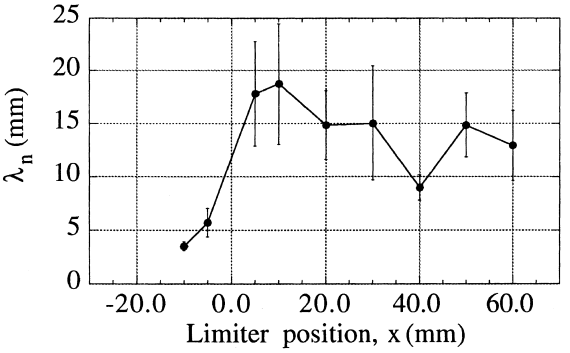

Fig. 5. Radial e-folding length of electron density in the limiter shadow as a function of the limiter position.

20% of the total ohmic input. The main contribution comes mainly from light impurities, N and B, released from the limiter, whose content in the plasma is observed to increase. The power loss increase is mainly accounted for by a corresponding increase of the radiated power. The transport power loss appears therefore to be unaffected by the presence of the limiter, at least in low current discharges. As far as the electron density is concerned, the two sets show comparable values in the core, whereas at the edge the presence of the limiter results in a relative increase of about 5%. The electron temperature profiles measured by a multipoint Thomson scattering system reveal that the on-axis electron temperature is slightly affected, whereas the T_e profiles at the edge indicate some plasma cooling, as shown in Fig. 3. The observed increase in H_α, associated to the decreasing of T_e, gives essentially unchanged particle influxes at the wall. Thus the main effect on the plasma seems to be limited to a localised increase of radiation losses in the boundary.

The radial decay of electron density and temperature measured by probe 1 and probe 3 in the shadow of the limiter are shown in Fig. 4, as a function of the insertion depth x defined in Fig. 2. Fig. 5 shows the radial profile of the electron density radial e-folding length λ_n at the edge; λ_n has been obtained from two-point interpolation of the densities measured by probes 1 and 3. A maximum occurs around $x \approx 10$ mm ($r/a \approx 0.98$), very close to the wall.

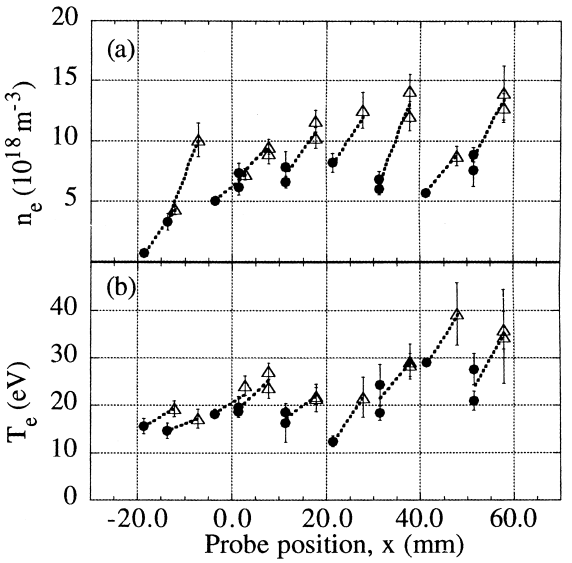

Fig. 4. Profiles of (a) electron density and (b) temperature in the limiter shadow in discharges at plasma current of 300–400 kA. Triangles refer to Langmuir probe 1; dots refer to Langmuir probe 3.

3. Diffusion coefficient at the plasma edge

Fig. 6 is an image taken with the probe inserted 30 mm in a 300 kA discharge. The bottom of the probe exposed to the electron drift side experiences the strongest interaction, as indicated by the intense emission. The latter is likely to be ascribed to the boron and to the nitrogen atoms sputtered or ablated from the probe surface. Once ionised the atoms flow downward almost poloidally, giving rise to an emitting stripe as large as the probe itself and covering a distance compatible with the estimated ionisation length of N II, that is, with the measured edge electron temperature in the shadow of the limiter (≈10–20 eV), of several hundreds of mm. The atoms ablated at the two lateral sides of the probe, once ionised, find their way also upward, displaying the two emitting stripes that delimit a dark region on the ion drift side, which instead reveals a zone of reduced interaction with the wall or equivalently a reduced hydrogen influx. All of the discharges at 300 kA show images as that shown in Fig. 6, hence the extension

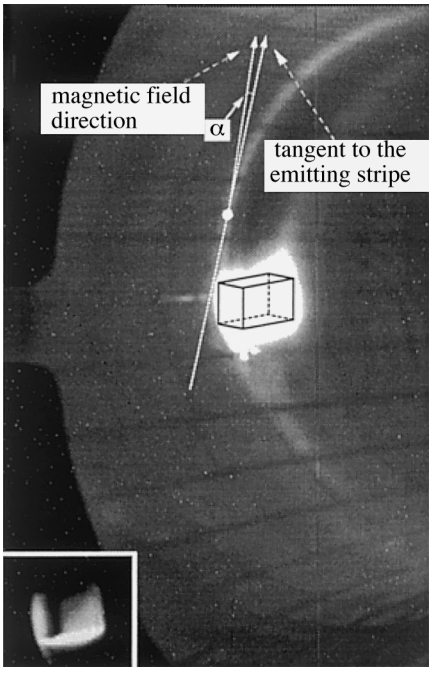

Fig. 6. CCD images (with different brightness) of the limiter inserted 30 mm into the plasma.

of the SOL is confirmed to be comparable or longer than $\pi a/2$. This value is assumed as the collection length of the limiter L_c.

The two nitrogen patterns appear to experience a toroidal drift in the same direction that can be explained in terms of the $\mathbf{E} \times \mathbf{B}$ velocity drift, which is found to be of the order of several km/s at the edge of RFX [8] and in accordance with the doppler shift measurement of C III [9]. As a consequence, the SOL regions in both drift sides do not appear to follow the geometry of the field lines, but they are slightly diverted, as illustrated in Fig. 6, where the angle α between the local magnetic field direction and the tangent to the emitting stripes is also shown.

A particle balance can be written for the SOL region of Fig. 2, considering the ion fluxes entering radially $\Gamma_{r_{in}}$ and toroidally Γ_t, as well as the ion fluxes outgoing radially $\Gamma_{r_{out}}$ to the wall and $\Gamma_\parallel = (1/2)nc_s$ leaving the region toward the probe surface:

$$L_c w(\Gamma_{r_{in}} - \Gamma_{r_{out}}) + 2L_c \int_0^x \Gamma_t \, dx + \int_{V_{SOL}} S_{ion} \, d^3x = w \int_0^x \Gamma_\parallel \, dx, \quad (1)$$

where c_s is the ion sound speed. An ion source term due to ionisation of neutrals $\int_{V_{SOL}} S_{ion} \, d^3x$ has been included in Eq. (1), where S_{ion} is the ion source per unit volume. This term includes ionisation of both slow neutrals desorbed from the wall and relatively fast neutrals sputtered from the limiter. The latter contribution is expected to be small, considering that the leading edge of the limiter on the ion drift side makes an angle of 45° with the magnetic field direction (Fig. 2). As a consequence, the large majority of the neutrals emitted from the limiter are ionised well beyond the LCFS, and therefore their contribution is not localized inside the SOL volume. A simple estimate, based on a cosine angular distribution of the sputtered and backscattered hydrogen neutrals indicates that only about 7% of the emitted fast neutrals are ionised inside the SOL, so that as a first approximation their contribution to the particle balance can be ignored.

Only the slow neutrals being the dominant source, the ion source per unit volume in the SOL can be written as

$$S_{ion} = \langle \sigma v \rangle n_n n, \quad (2)$$

where n is the local electron density and n_n is the hydrogen neutral density. The latter can be evaluated by assuming a perfect balance between the flux of impinging ions, whose density decays exponentially in the SOL, and the flux of released neutrals, as given in [10]

$$n_n v_n = D \frac{n}{\lambda_n} \exp(-x/\lambda_n), \quad (3)$$

where D is the radial particle diffusion coefficient at the LCFS and v_n is the average velocity of the neutral atoms released from the wall. Using an exponential radial decay of electron density in the SOL, the ion source in Eq. (1) can be rewritten as

$$\int_{V_{SOL}} S_{ion} \, d^3x \approx \frac{L_c w}{\lambda_{iz}} Dn(1 - \exp(-x/\lambda_n)) \exp(-x/\lambda_n), \quad (4)$$

where $\lambda_{iz} = v_n/n\langle \sigma v \rangle$ is the ionisation length for hydrogen neutrals. The images of the CCD camera indicate that this term should not be the dominant one in Eq. (1), since the wide darker region extending along the ion drift side of the SOL is evidence of the local absence of an appreciable neutral-ion transition rate. The following parameters are assumed in the SOL: $T_e \approx 20$ eV with uniform profile, $n \approx 10^{19}$ m^{-3}, $\langle \sigma v \rangle \approx 10^{-14}$ m^3/s [11], $v_n \approx 5$ km/s (low energy H neutrals), giving $\lambda_{iz} \approx 50$ mm, i.e. comparable to l, so that Eq. (4) is applicable throughout the range of variation of x.

The radial fluxes $\Gamma_{r_{in}}$, $\Gamma_{r_{out}}$ and the toroidal flux Γ_t can be evaluated by using Fick's law:

$$\Gamma_{r_{in}} = D\nabla n \cong D\frac{n}{\lambda_n}, \qquad \Gamma_{r_{out}} \cong D\frac{n}{\lambda_n} \exp\left(-\frac{x}{\lambda_n}\right),$$
$$\Gamma_t \cong D_t \frac{n}{\lambda_{nt}}, \quad (5)$$

where D_t and λ_{nt} are respectively the diffusion coefficient and the ion density decay lengths in the limiter shadow in the toroidal direction. A rough estimate for D_t can be deduced from the broadening of the N II ionisation stripes along the borders of the SOL region as seen from the CCD camera. It appears consistent with a value of the order of 10 m^2/s, i.e. of the same order of the expected value of D [8]; hence it is assumed $D_t \approx D$. An indication about the value of λ_{nt} could be drawn from the toroidal dependence of the H_α emission, but from the images it is rather difficult to deduce quantitative figures. It appears reasonable to assume $\lambda_{nt} \approx \lambda_n$ [12].

Using Eqs. (4) and (5) and integrating, the balance Eq. (1) can be rewritten as

$$L_c D\left[\frac{1-\exp(-x/\lambda_n)+\frac{2x}{w}+\frac{\lambda_n}{\lambda_{iz}}(1-\exp(-x/\lambda_n))\exp(-x/\lambda_n)}{(1-\exp(-x/\lambda_n))}\right] = \frac{\lambda_n^2 c_s}{2}. \quad (6)$$

The term in square brackets in Eq. (6) is an analytical function of x, which takes on values between 1.3 and 2 in the interval from 0 to 60 mm. Calling this function $M(x)$, the following expression for D is finally obtained:

$$D = \frac{\lambda_n^2 c_s}{2M(x)L_c}. \quad (7)$$

By using the measured λ_n values given in Fig. 6, the diffusion coefficient derived from the SOL balance is compared in Fig. 7 with that derived from electrostatic turbulence [6]. An effective perpendicular diffusion coefficient D_{es} has been deduced from the ratio between the radial flux measured via the cross-correlation between density and electric field fluctuations and the local density gradient [1,6]. It is found that D tracks D_{es} with a maximum close to the wall and a minimum in correspondence to a maximum in the $\mathbf{E}\times\mathbf{B}$ velocity shear observed at the edge [1,6]. In the same figure the values derived from the Bohm estimate are also reported, showing that in the plasma at $r/a \approx 0.95$ the experimental estimate corresponds to Bohm diffusion, whereas it seems to be larger close to the wall and smaller inside the plasma.

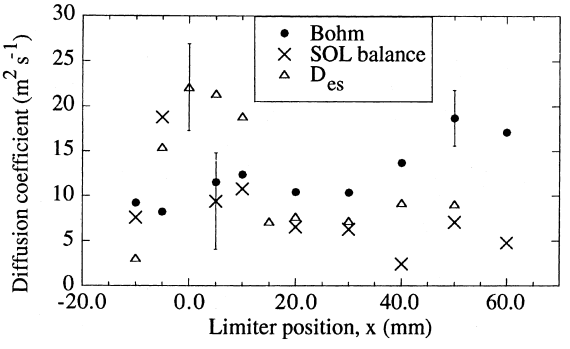

Fig. 7. Diffusion coefficient derived from SOL balance and obtained from electrostatic fluctuations, compared with Bohm value. Typical error bars are shown.

The model can be applied also to the region inside the porthole (points at $x < 0$ in Fig. 7), by substituting $M(x) \approx 1$ in Eq. (7), since that region is a simple SOL. The measured λ_n appear to be consistent with the values measured inside the porthole by probes mounted in a different housing support made of graphite [13]. Using Eq. (7), with the well defined connection length in the prothole ($L_c \sim 40$ mm in this case) and $\lambda_n \approx 5$ mm, a reasonably good matching is obtained between the particle diffusion coefficient evaluated at $x < 0$ and at $x > 0$. The measured diffusivity confirms the value of $D \approx 10$ m^2/s found for carbon impurity from Langmuir and deposition probes [13].

4. Conclusions

The effective perpendicular diffusivity derived from a simple particle balance in the SOL generated by an insertable limiter in the edge of RFX is consistent with that derived from the electrostatic transport, confirming that most of the particle flux at the edge is driven by electrostatic turbulence. These values are both comparable to the Bohm diffusion coefficient. Comparisons with independent estimates derived from interferometer measurements and particle diffusion simulation in RFX are both in agreement with the data presented herein. The impurity diffusion coefficient results in the SOL of the porthole are comparable to those of the main plasma.

References

[1] V. Antoni, Plasma Phys. Control. Fusion 39 (1997) B223.
[2] G. Rostagni, Fusion Eng. Des. 25 (1995) 301–313.
[3] L. Garzotti et al., Proc. 24th Eur. Conf. on Control. Fusion and Plasma Phys., Berchtesgaden, vol. 21A, Part I, EPS, 1997, p. 313.
[4] F. Gnesotto, P. Sonato, W.R. Baker, A. Doria, F. Elio, M. Fauri, P. Fiorentin, G. Marchiori, G. Zollino, Fusion Eng. Des. 25 (1995) 335.
[5] V. Antoni, E. Martines, M. Bagatin, D. Desideri, G. Serianni, Nucl. Fusion 36 (1996) 435.
[6] V. Antoni, R. Cavazzana, E. Martines, G. Serianni, M. Bagatin, D. Desideri, M. Moresco, E. Spada, L. Tramontin, these Proceedings.
[7] R. Pasqualotto, R. Pugno, M. Valisa, L. Carraro, M.E. Puiatti, F. Sattin, P. Scarin, Plas. Dev. Op. 5 (1998) 287.
[8] V. Antoni, R. Cavazzana, D. Desideri, E. Martines, G. Serianni, L. Tramontin, Phys. Rev. Lett. 80 (1998) 4185.
[9] L. Carraro, M.E. Puiatti, F. Sattin, P. Scarin, M. Valisa, Plasma Phys. and Control. Fusion, to be published.

[10] P.C. Stangeby, G.M. McCracken, Nucl. Fusion 30 (1990) 1225.
[11] G.S. Voronov, Atomic Data Nucl. Data Tables 65 (1997) 1.
[12] G.F. Matthews, P.C. Stangeby, J. Phys. D: Appl. Phys. 22 (1989) 644.
[13] V. Antoni, M. Bagatin, H. Bergsåker, G. Della Mea, D. Desideri, E. Martines, V. Rigato, L. Tramontin, S. Zandolin, J. Nucl. Mater. 220–222 (1995) 650.